International Journal of Nanomedicine

Dovepress
open access to scientific and medical research

Open Access Full Text Article

ORIGINAL RESEARCH

Hairpin DNA-Based Nanomaterials for Tumor Targeting and Synergistic Therapy

Lingling Shan[1], Yudie Li[1], Yifan Ma[2], Yang Yang[1], Jing Wang[1], Lei Peng[1], Weiwei Wang[1], Fang Zhao[1], Wanrong Li[1], Xiaoyuan Chen[3–6]

[1]Institute of Pharmaceutical Biotechnology, School of Biology and Food Engineering, Suzhou University, Suzhou, People's Republic of China; [2]Wuya College of Innovation, Shenyang Pharmaceutical University, Shenyang, People's Republic of China; [3]Departments of Diagnostic Radiology, Chemical and Biomolecular Engineering, and Biomedical Engineering, Yong Loo Lin School of Medicine and College of Design and Engineering, National University of Singapore, Singapore, Singapore; [4]Clinical Imaging Research Centre, Centre for Translational Medicine, Yong Loo Lin School of Medicine, National University of Singapore, Singapore, Singapore; [5]Nanomedicine Translational Research Program, NUS Center for Nanomedicine, Yong Loo Lin School of Medicine, National University of Singapore, Singapore, Singapore; [6]Institute of Molecular and Cell Biology, Agency for Science, Technology, and Research (A*STAR), Singapore, Singapore

Correspondence: Xiaoyuan Chen; Lingling Shan, Email chen.shawn@nus.edu.sg; ntlinger-300@163.com

Background: While nanoplatform-based cancer theranostics have been researched and investigated for many years, enhancing antitumor efficacy and reducing toxic side effects is still an essential problem.

Methods: We exploited nanoparticle coordination between ferric (Fe^{2+}) ions and telomerase-targeting hairpin DNA structures to encapsulate doxorubicin (DOX) and fabricated Fe^{2+}-DNA@DOX nanoparticles (BDDF NPs). This work studied the NIR fluorescence imaging and pharmacokinetic studies targeting the ability and biodistribution of BDDF NPs. In vitro and vivo studies investigated the nano formula's toxicity, imaging, and synergistic therapeutic effects.

Results: The enhanced permeability and retention (EPR) effect and tumor targeting resulted in prolonged blood circulation times and high tumor accumulation. Significantly, BDDF NPs could reduce DOX-mediated cardiac toxicity by improving the antioxidation ability of cardiomyocytes based on the different telomerase activities and iron dependency in normal and tumor cells. The synergistic treatment efficacy is enhanced through Fe^{2+}-mediated ferroptosis and the β-catenin/p53 pathway and improved the tumor inhibition rate.

Conclusion: Harpin DNA-based nanoplatforms demonstrated prolonged blood circulation, tumor drug accumulation via telomerase-targeting, and synergistic therapy to improve antitumor drug efficacy. Our work sheds new light on nanomaterials for future synergistic chemotherapy.

Keywords: DNA nanomaterials, targeting, imaging, synergistic therapy

Introduction

An average of 13 nanomaterials have been approved for clinical antitumor therapy every five years since the mid-1990s.[1,2] This situation has extensively promoted the rapid development of nanomaterials. DNA nanostructures have the advantages of high programmability, addressability, modifiability, biocompatibility, and nontoxicity and have been widely used as drug delivery systems in treating malignant tumors.[3,4] However, multifunctional polymeric DNA nanodrug delivery systems have shortcomings in therapeutic applications, such as enzyme degradation, protein adsorption, and unclear metabolic pathways.[5,6] Therefore, numerous researchers have used combinations of DNA nanomaterials with other nanoparticles or polymer compounds, such as gold nanoparticles,[7] metal-organic frameworks (MOFs),[8] chitosan,[9] and polylysine,[10] to overcome the limitations of DNA nanomaterials.[11,12] As a result, the prepared DNA nanodrug delivery systems are polymers with complicated particle structures that are difficult to metabolize and have preparation and purification processes that are difficult to simplify.

Since telomerase is specifically highly expressed in approximately 85% of tumor cells but poorly expressed in normal cells, it can target tumors.[13,14] Thus, telomerase-targeting DNA nanodrug delivery systems can be designed to load anticancer chemotherapy drugs and facilitate the recognition of tumor cells or tissues. A certain number of DNA fragments, such as 10–20 base DNA fragments, has recently been found to be rich in A/C base pairs and can form DNA nanostructures

Received: 10 March 2024
Accepted: 29 May 2024
Published: 12 June 2024

Graphical Abstract

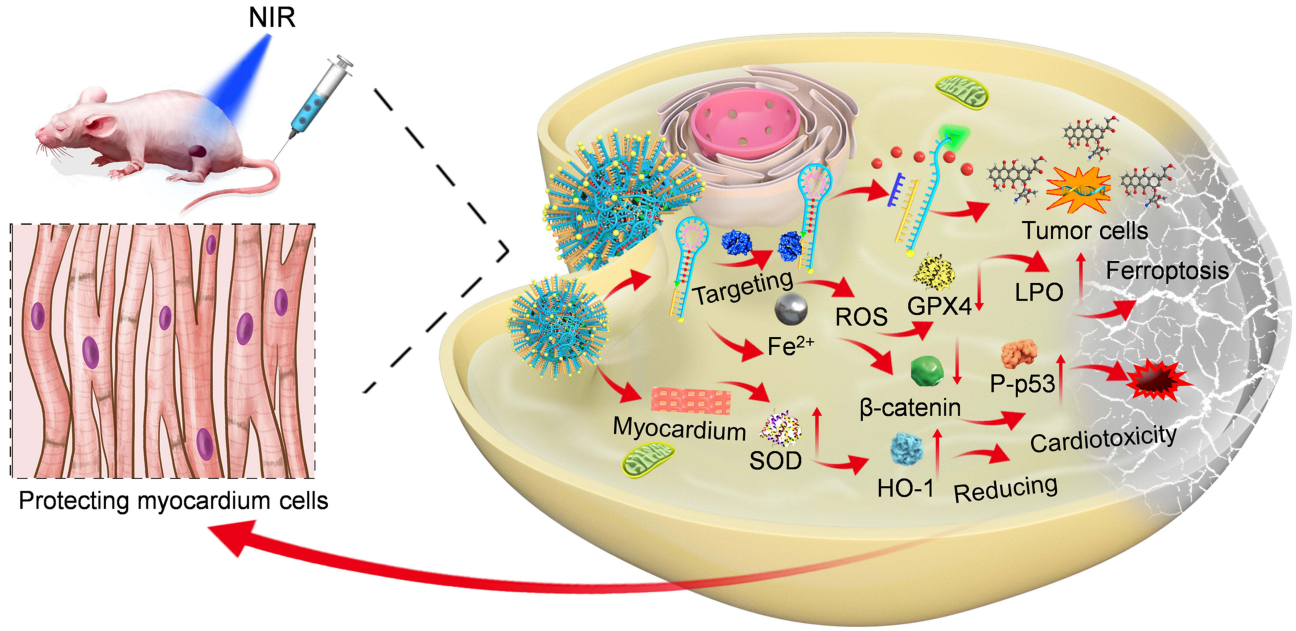

with ferric (Fe^{2+}) ions at high temperatures.[15,16] The preparation of these nanostructures requires a reaction at 95 °C for three hours. Reaction at high temperatures inevitably affects functional DNA activity and chemotherapy drug structure and functions.[17,18] The prepared nanoparticles also have problems, such as uncontrollable large sizes and poor dispersion.[19,20] Therefore, the challenges and areas of focus for the current research on green DNA nanodrug delivery systems are the development of simple and efficient nondestructive preparation methods that ensure DNA activity, stability, targeting, and safety, as well as the investigation of their mechanisms of action and metabolic pathways in vivo.

Anthracyclines, such as doxorubicin (DOX) and daunorubicin, are first-line anticancer drugs that can insert into G-C-rich double helix regions.[21,22] Their stability provides many possibilities for customizing DNA nanostructures as drug delivery systems. The construction of DNA-DOX nanodrug delivery systems is usually divided into two methods: DNA origami[23,24] and DNA module assembly.[25,26] DOX nanoparticle drug carriers constructed via the DNA origami method exhibit uniform shapes and sizes and high complexity, require numerous short DNA strands, and have high synthesis costs.[27] DNA module assembly presents poor shape and size control, resulting in poor nanoparticle dispersion and excessively long nanoparticles, which cannot be used as drug carriers.[28] Designed the stem of a DNA hairpin structure that targets tumor telomerase as a G-C base pair that can carry the chemotherapy drug DOX. Studies prepared a DNA-DOX structure by coupling the 3′ end of the sulfhydryl group of DNA on the surfaces of gold nanoparticles to achieve targeted drug delivery.[22] However, preparing this nanodrug delivery system involves coupling the DNA hairpin structure on the surface of gold nanoparticles, and the resulting drug loading rate was low. In vivo, the DNA hairpin structure exhibited shortcomings, such as easy catabolism by enzymes.[21] Other literature used the principle of coordination between target DNA-DOX and Fe^{2+} to wrap DNA-DOX on the surface of MOFs at high temperatures and form nanoparticles with complex structures. Despite their improved DOX loading capacities, the scientific problems of the above DNA-DOX nanodrug delivery systems remain unsolved.[29] The G-C base pair can carry a DOX carrier in the telomerase-targeting DNA hairpin structure stem. The loop part of the hairpin structure (single chain) is rich in A bases. The N-7 of A and coordination between DOX and Fe^{2+} can be exploited to self-assemble DNA nanodrug delivery systems.[30] This preparation method is simple, efficient, and nondestructive, but it also can improve the drug loading and active targeting of nanomedical drug delivery systems based on DNA-DOX. Most importantly, tumor cells show an increased iron demand during tumor growth compared with normal, non-cancer cells. Thus, Fe^{2+}-coordinated nanoparticles

can catalyze tumor cell necrosis, referred to as the ferroptosis pathway, a new type of cell death accompanied by a large amount of iron accumulation and lipid peroxidation during the cell death process.[31]

Based on previous studies, molecular beacons, coordination chemicals, and DNA nanotechnology were combined to synthesize DNA-based nanoparticles. In these particles, DOX was inserted into the G-C base pair of DNA-DOX, a tumor telomerase-targeting DNA hairpin structure. Meanwhile, using the molecular beacon principle, namely, coordination between Fe^{2+} and DNA-DOX, the 5′ and 3′ ends of DNA were labeled with 6-Carboxyfluorescein (6-FAM) and Dabcyl quenched groups. The Dabcyl-labeled 3′ terminal region is hybridized with telomerase primers, and the 6-FAM-labeled 5′ terminal region possesses the telomeric repeats sequences. U87MG (malignant glioma) cells were applied as a model because of their high telomerase activity and iron dependency. In vitro and in vivo studies studied the targeting, toxicity, and synergistic therapeutic effects of the nanoplatform.

Methods

Assembly of Hairpin DNA@DOX-Fe^{2+} Nanoparticles

First, overnight, hairpin DNA (Supplementary Material, 100 nm) was activated at room temperature and incubated with the same concentration of primers for 12 h. A total of 0.1 mL of DOX hydrochloride (3 mg, 0.005 mmol) was reacted with hairpin DNA-primer complexes in ddH_2O overnight to prepare DNA-DOX. Next, aqueous solutions of $FeCl_2$ (50 μL, 10 mg/mL) were slowly added to the DNA-DOX mixture and stirred overnight at room temperature to obtain BDDF NPs. Finally, dialysis removed excess DNA, DOX, and $FeCl_2$ from the mixture (20,000 MWCO). DNA and DOX concentrations were evaluated by using HPLC. BDDF NPs were studied through in vitro and in vivo experiments.

Targeting of BDDF NPs in Tumor Cells

The tumor cell line U87MG (human primary glioblastoma cells) and normal cell line AC16 (human myocardial cells) were cultivated in a confocal cell plate at a density of 1×10^5/well for 1, 3, and 5 h. Medium with BDDF NPs (6.9 μM DOX) was added to the U87M cells. The targeting of BDDF NPs in tumor cells was determined through confocal microscopy and flow cytometry. Gel electrophoresis was used to confirm the occurrence of the "on" state when the hairpin DNA and primer were combined with telomerase.

In vitro Evaluation of Telomerase Activities and ROS and LPO Levels

U87MG and AC16 cells were plated in six-well plates at a density of 1×10^5, added with medium containing BDDF NPs (6.9 μM DOX), and incubated for another 5 h. Telomerase activities and LPO levels in all cells were measured by using kits. Finally, all samples were dissolved and subjected to HPLC. DCF was used to detect the intracellular ROS concentration in U87MG cells based on fluorescence through confocal imaging and flow cytometry. Western blot analysis with the GPX4 protein in AC16 cell.

In vitro Toxicity of BDDF NPs

The cytotoxicity of BDDF NPs was assessed through the MTT test. AC16 and U87MG cells were cultured in a 96-well plate at a 5×10^3/well density and incubated at 37 °C and 5% CO_2. After 24 h of culture, each well was added with Fe^{2+}(34.5μM), Fe^{2+}-DOX, DNA-DOX, and BDDF NPs at the same concentration as DOX (6.9 μM) and incubated for 48 h at 37 °C and 5% CO_2. The medium was replaced with 100 μL of fresh medium and 10 μL of MTT (5 mg mL^{-1} in PBS) and incubated for another 4 h. The supernatant was then removed, and DMSO (100 μL) was added to each well. Absorbance was measured by a microplate reader at 570 nm.

Analysis of Cell Apoptosis Induced by BDDFP NPs

The apoptosis of U7MG tumor cells was studied through qualitative and quantitative analyses. U87MG cells were seeded in a confocal plate at a density of 10^5/well, cultured at 37 °C for 24 h, added with culture media containing BDDF NPs at the same concentration as DOX (6.9 μM), and co-incubated for 24 and 48 h by using Dead Cell Apoptosis Kit with

Annexin V PE and SYTOX™ Green Kit. Quantitative apoptosis results were obtained by using flow cytometry. The qualitative imaging of cells was performed through confocal microscopy.

In vivo Acute and Cardiac Toxicity Studies

The in vivo acute toxicity of BDDF NPs was evaluated in BALB/c mice. Fifteen BALB/c mice were randomly divided into three groups (age = 5 weeks, weight = 21 g, n = 5 per group), which were treated with PBS (control group), DOX (2 mg kg^{-1}), or BDDF NPs (DOX, 2 mg kg^{-1}). 200 μL of PBS, DOX, and BDDF NPs were intravenously injected into the mice in each group. At 1, 3, and 7 days postinjection, blood was collected from the eye socket for the measurement of biochemical parameters, such as aspartate aminotransferase (AST), alanine aminotransferase (ALT), creatine kinase (CK), and creatine kinase-MB (CK-MB). All mice were sacrificed seven days postinjection, and their liver tissues were sectioned for H&E analysis. The SOD activities of heart tissues were tested with a kit, and HO-1 protein expression was evaluated through Western blot analysis.

Pharmacokinetics Studies

U87MG tumor-bearing mice were randomly divided into two groups (n = 4 per group) and intravenously injected with 200 μL of DOX and BDDF NPs at the same concentration as DOX (2 mg kg^{-1}). At 10 min and 0.5, 1, 2, 4, 8, 24, and 48 h postinjection, four mice from each group were sacrificed, and 300 μL of blood was collected via terminal cardiac puncture under anesthesia.[32] Tumor tissue was further studied using an LPO kit and Western blot analysis with the GPX4 protein.

In vivo Targeting Imaging Studies

BDDF NPs were labeled with ICG conjugated with 5-hydroxydopamine at a ratio of 1:3.[33] Mice with xenograft U87MG tumors were intravenously injected with 200 μL of BDDF NP solution with 2 mg kg^{-1} DOX. Fluorescent imaging was conducted with an NIR system (PerkinElmer Inc.) at 1, 4, 8, 12, 24, and 48 h postinjection.

In vivo Antitumor Therapy

U87MG tumor-bearing nude mice were randomly assigned to three groups (n = 5 per group): (A) PBS buffer (pH 7.4, control), (B) free DOX (2 mg kg^{-1}), and (C) BDDF NPs (DOX dose of 2 mg kg^{-1}). All mice were injected through tail vein injection three times every other day. Antitumor therapeutic effects and toxicities were estimated in U87MG tumor-bearing nude mice by measuring the tumor volume and body weight every other day. The heart, liver, and tumor tissues from each group were excised for pathology, and typical proteins, including β-catenin and p53, were further analyzed through Western blot analysis. We further assessed tumor tissues by using immunohistochemical techniques.

Statistical Analysis

Statistical analysis was performed using the Student's *t*-test. Statistical significance was assigned as follows: $*P < 0.05$, significant; $**P < 0.01$, moderately significant; and $***P < 0.001$, highly significant.

Results

Characterization of the DNA Nanodrug Delivery System

As illustrated in Figure 1a, the hairpin stem mainly comprised seven G-C base pairs into which DOX can be inserted. The hairpin ring was enriched with the A base group that coordinated with Fe^{2+} ions to assemble BDDF NPs (molecular beacon Fe^{2+}-DNA@DOX). First, the structure of the hairpin DNA and primer was identified through LC-MS (Figures S1 and S2). The TEM images of BDDF NPs were displayed in Figure 1b, which revealed that the as-prepared BDDF NPs presented excellent monodispersity and circular-like shape morphology. Dynamic light scattering showed that the size of BDDF NPs was 61.2 ± 7 nm (Figure 1c). The zeta potentials of BDDF NPs have been measured and provided in Figure S3. The NPs are negatively charged (~18.2 mV) owing to the hairpin DNA structures of nanoparticles, consistent with the previous report.[17] Interestingly, in this circular-like shape, nanoparticles, DOX were embedded into the G-C base pairs in hairpin DNA to form the core of BDDF NPs, thus reducing toxicity to normal cells or tissues. The release of DOX from BDDF NPs increased as

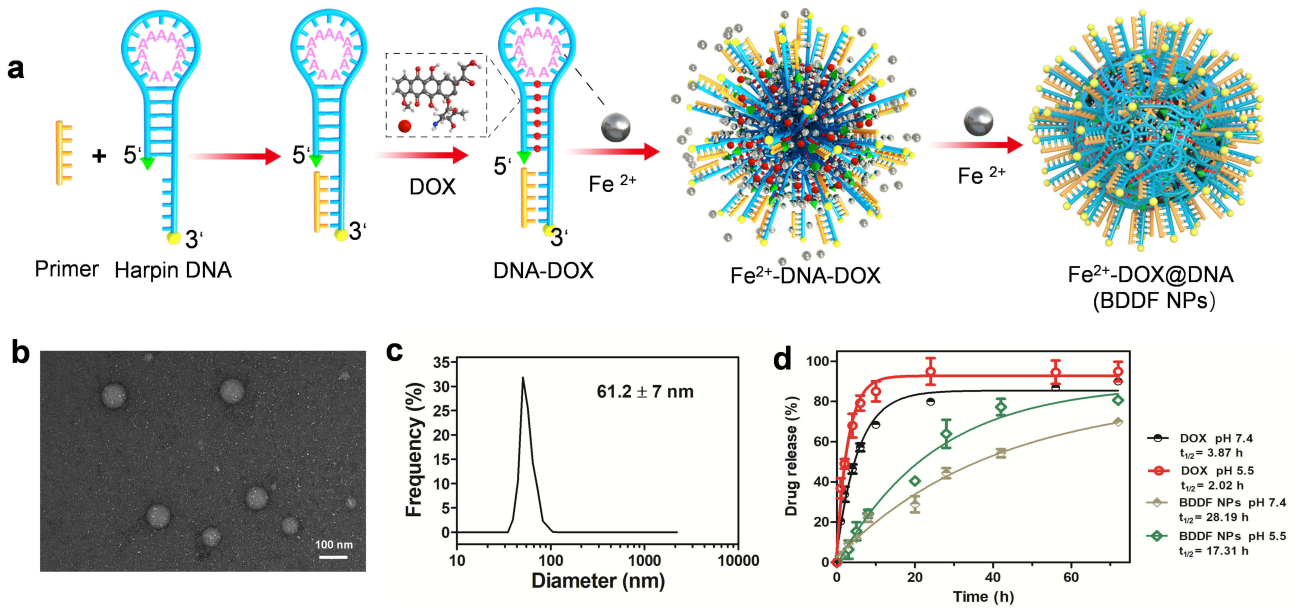

Figure 1 Scheme and characterization of nanoparticles. (**a**) Schematic illustration of the synthetic procedure of BDDF NPs. (**b**) TEM images and (**c**) DLS of BDDF NPs. (**d**) HPLC analysis for in vitro DOX release from free DOX, BDDF NPs in buffer solutions (pH = 7.4, 5.5). n = 3, mean ± s.d.

the pH changed from 7.4 to 5.5. Therefore, DOX-loaded Fe^{2+}-DNA drug delivery occurred with a pH-controlled release profile. DOX concentrations were determined through HPLC (Figure 1d and S4). We measured the loading of DOX and Fe^{2+} using HPLC and UV-vis methods (Supplementary Material). The results showed that the loading of DOX in BDDF NP was at 57%, and the loading of Fe^{2+} was at 45%. The mole ratio of the reaction was 1: 5 (DOX: Fe^{2+}). (Figures S4 and S5)

In vitro Targeting, Telomerase Activities, and ROS and LPO Levels

The cellular uptake of BDDF NPs was verified through confocal microscopy and flow cytometry. U87MG tumor cells were cultured with BDDF NPs for 1, 3, and 5 h. The confocal microscopy images in Figure 2a and d illustrated that BDDF NPs were taken up by cells. In the meantime, flow cytometry data showed that cell uptake increased with the increase in incubation time (Figure 2b and c). When the incubation time was from 1 h to 5 h, cell nuclei accumulated the red fluorescence of DOX and became surrounded by green fluorescence, suggesting that hairpin DNA was released from BDDF NPs into the cytoplasm.

Intracellular ROS levels were determined using a ROS indicator (DCFH-DA). The enhancement in the green fluorescence signal of ROS in the presence of $FeCl_2$, DOX, and BDDF NPs (Figure 2d) indicated that BDDF NPs showed high efficiency in promoting the elevation of ROS levels. Fe^{2+} coordination-based BDDF NPs could increase the Fe^{2+}-mediated Fenton effect to enhance ROS levels in U87MG cells.

Telomerase activities and LPO levels were evaluated by using tumor and normal cells. Figure 2e and f illustrated a significant difference between tumor and normal cells: tumor cells showed high telomerase activities and LPO levels under different treatments, whereas normal cells had little telomerase activity and low LPO levels. Tumor cells displayed a different ferroptosis pathway compared with normal cells.[31,34] The gel electrophoresis results in Figure 2g confirmed that telomerase was bound with the hairpin DNA primer to maintain the hairpin DNA in an "on" state and exhibited green fluorescence (Supplementary Material).

Cytotoxicity, Cell Apoptosis, and GPX4/β-Catenin/p-53 Protein Studies of BDDF NPs

The in vitro cytotoxic effect of BDDF NPs was evaluated using tumor (U87MG) and normal (AC16) cells. As shown in Figures 3a and b, DOX, DNA-DOX, and BDDF NP exerted dose-dependent cytotoxic effects on the two cell lines. In the U87MG tumor cells, the BDDF NPs presented more than 88% inhibition ratios. By contrast, the DOX group inhibited a maximum of 65% of U87MG cells. The cytotoxicity of free Fe^{2+} and Fe^{2} -DOX shown the ferrous ions had lower

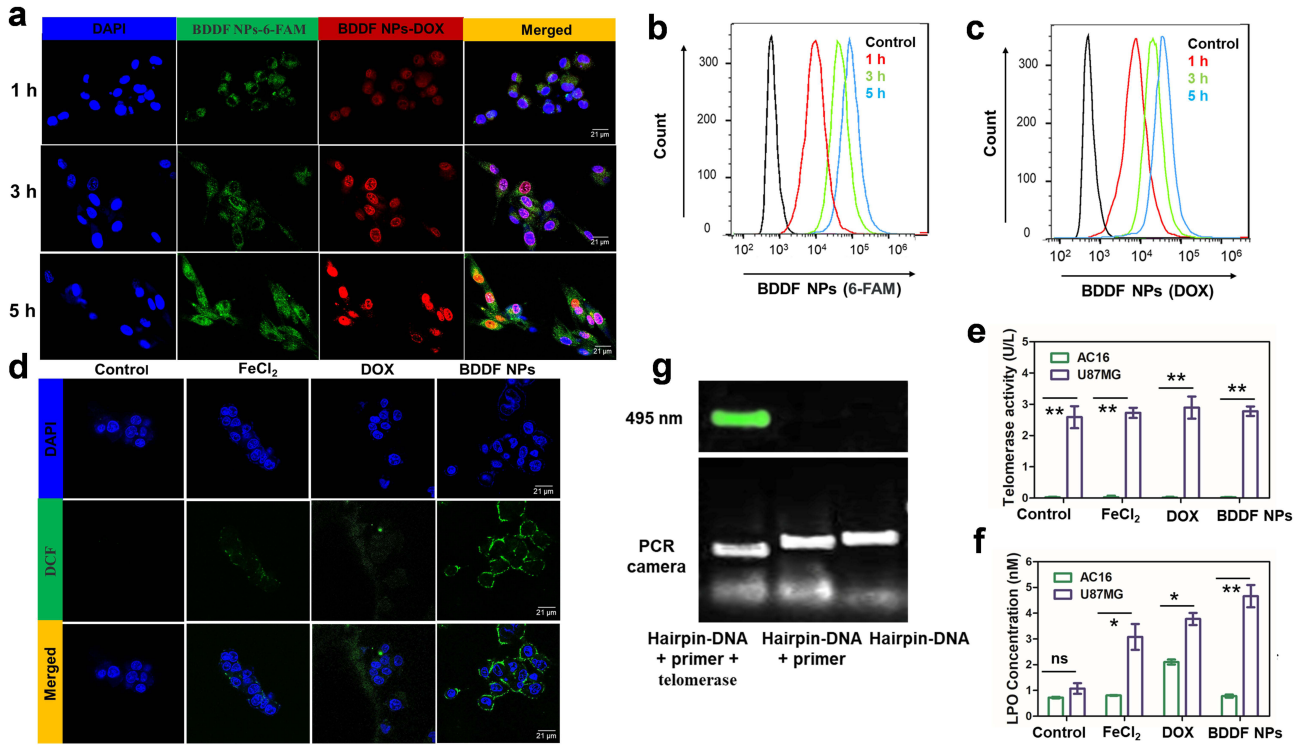

Figure 2 Cell uptake and telomerase activity. (**a**) The confocal microscopy images of U87MG cell uptake following various incubation times. The green, blue, and red fluorescence were from the cell cytoplasm (harpin DNA-6 AM), nucleus (DAPI), and DOX, respectively. Scale bars are 25 μm. (**b** and **c**) The flow cytometric analyses of U87MG cell uptake. (**d**) Detection of intracellular ROS using a ROS indicator, DCFH-DA, in U87MG cells. (**e**) Telomerase activities at 5 h after different treatments in U8MG and AC16 cells. (**f**) LPO levels at 5 h after various treatments in U87MG and AC16 cells. (**g**) Gel electrophoresis further confirmed the telomerase bonded with the hairpin DNA primer to maintain the hairpin DNA in an "on" state and exhibited green fluorescence under 495 nm telomerase bonded with the hairpin DNA primer to retain the DNA hairpin in an "on" state and exhibited green fluorescence. *$P < 0.05$; **$P < 0.01$.

cytotoxicity in AC16 cells than in U87MG tumor cells. Similarly, the IC_{50} value of BDDF NPs was 0.29 μM against U87MG, which was lower than DOX, and 23.7μM against AC16 cells, higher than DOX, DNA-DOX, and Fe^{2+}-DOX groups. The IC_{50} of Fe^{2+} was 45.08 μM against AC16 cells, which was higher two times than U87MG cells (Figure 3c). The results showed that Fe^{2+} had no cytotoxicity in normal cells, and the iron uptake in tumor cells was higher than in normal cells. That is because tumor cells are iron-dependent during growth compared to normal cells.

This BDDF NPs nanodrug delivery system has tumor telomerase-targeting hairpin DNA, which lowers cytotoxicity in normal cells. The half-maximal inhibitory concentration of free DOX was higher than that of BDDF NPs, suggesting that BDDF NPs have excellent tumor cell-targeting effects (Figure 3c). Importantly, BDDF NPs displayed lower inhibitory effects on AC16 normal cells than on U87MG tumor cells at the same doses, likely due to the low telomerase activities in the normal cells.[35] The apoptosis of U87MG cells was investigated through qualitative (confocal) and quantitative (flow cytometry) analyses. As illustrated in Figures 3d and e, S6, the quantitative results verified that the percentage of apoptotic cells (early [Q2] and late [Q4] apoptosis) increased by incubation time. BDDF NPs resulted in the highest percentage of apoptotic cells (Q4) after 48 h of incubation. All proteins in U87MG cells were analyzed through Western blot analysis (Figures 3f and g). In contrast to DOX, the BDDFF NPs significantly inhibited β-catenin and increased the protein levels of P-p53/p53. This finding further demonstrated that BDDF NPs exerted synergistic cell apoptosis effects. GPX4 protein, the representative protein in the ferroptosis pathway, was barely expressed. On the contrary, the GPX4 protein had higher expression in AC16 cell lines with BDDF NP incubation (Figure S7) and proved the different ferroptosis pathways between the tumor cells and normal cells. All results indicated that the BDDF NPs presented low cytotoxicity against normal cells and enhanced cytotoxicity against U87MG tumor cells via the β-catenin/p-53 and ferroptosis pathways.

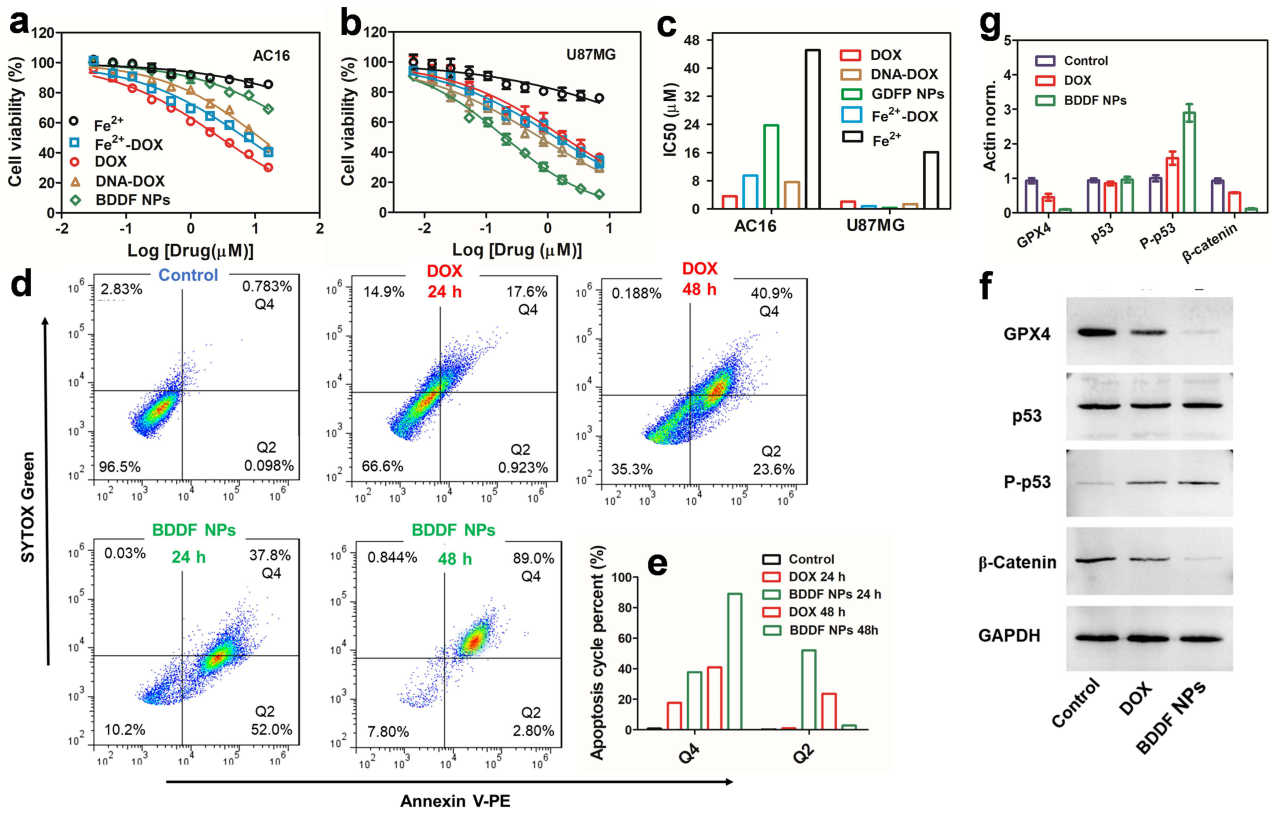

Figure 3 Cell viability, apoptosis, and Western blotting analysis. (**a** and **b**) Cell viabilities of AC16 cells (**a**) and U87MG cells (**b**) following different treatments at 48 h. (**c**) The IC_{50} values of free DOX, DNA-DOX, Fe^{2+}, Fe^{2+}-DOX, and BDDF NPs for AC16 and U87MG cells. (**d**) The cell apoptosis of U87MG cells following incubation with DOX, BDDF NPs for 24 and 48 h, and the apoptosis cycle percent in Q2 and Q4 zones (**e**). (**f** and **g**) Western blotting results of GPX4, P-p53, p-53, and β-Catenin expression from U87MG cells after 48 h incubation with DOX and BDDF NPs.

Acute Cardiac Toxicity Studies

In this work, a DNA nanodrug delivery system was designed based on BDDF NPs that target tumor telomerase to reduce DOX retention in the heart, thereby simultaneously reducing DOX-mediated cardiotoxicity and enhancing synergistic chemotherapeutic effects. We evaluated the acute toxicity of DOX and BDDF NPs in vivo. Blood was collected from the three groups to measure blood biochemistry parameters at 1, 3, and 7 days postinjection. As shown in Figures 4a–d, the free DOX group exhibited severe cardiotoxicity and hepatotoxicity with significantly increased biochemistry parameters, such as CK, CK-MB, AST, and ALT. Meanwhile, SOD activity and HO-1 protein expression were lower in the DOX group than those in the BDDF NP group (Figure 4e and f). By contrast, all BDDF NP group blood parameters were within the normal range. The above results proved that the tumor telomerase-targeting BDDF NPs could significantly reduce DOX-mediated cardiac toxicity. The images of the pathological heart tissue sections from the DOX and BDDF NP groups further verified that free DOX caused slight heart damage. No remarkable histological signs were observed under treatment with BDDF NPs (Figure 4g).

Optical Imaging and Biodistribution and Pharmacokinetic Studies

In vivo NIR imaging was performed by using BDDF NPs labeled with ICG-5-hydroxydopamine.[33] ICG-labeled BDDF NPs were injected into U87MG tumor-bearing mice via the tail vein. We acquired images at 1, 4, 8, 12, 24, and 48 h postinjection. The quantitative NIR images are provided in Figure 5b. BDDF NPs quickly accumulated at the tumor site at 4 h, and NIR imaging fluorescence signals peaked at 12 h with a T/N ratio of 10.56 ± 0.554. At 48 h postinjection, the fluorescence intensity of BDDF NPs in tumors remained as high as 6.67 ± 0.332 (T/N). In addition, ImageJ software analyzed the T/N levels of major organs and tumors at different time points (Figure 5c). In vivo NIR imaging from 4 h to 12 h, the fluorescence signal from the tumor tissues was considerably more robust than that from other organs. Moreover,

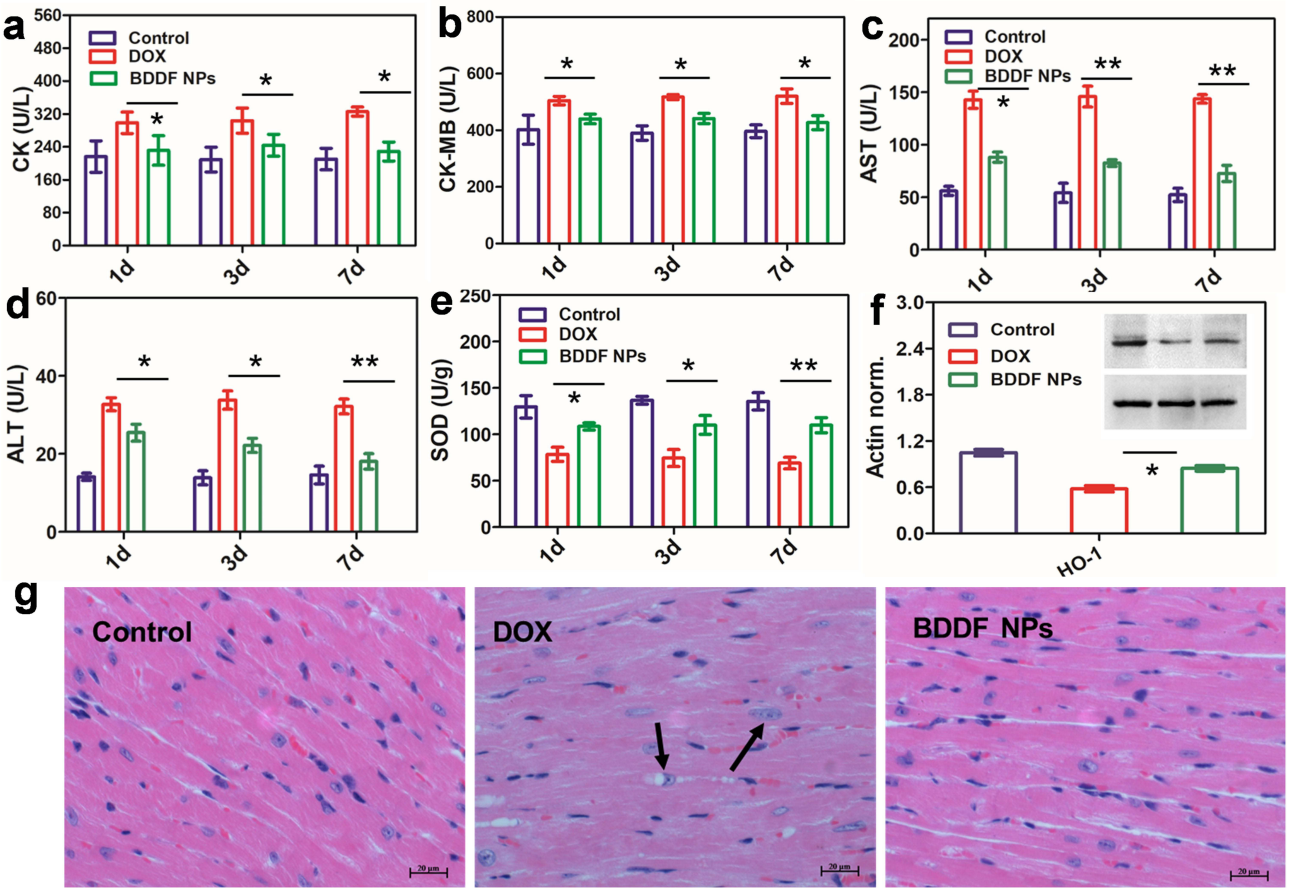

Figure 4 Acute toxicity and cardiac toxicity analysis. Blood biochemistry test of CK (**a**), CK-MB (**b**), AST (**c**), and ALT (**d**) after various treatments (n = 4). *$P < 0.05$; **$P < 0.01$. (**e**) The activity of SOD from heart tissues after various treatments (n = 3). *$P < 0.05$; **$P < 0.01$. (**f**) Western blotting results of HO-1 expression from heart tissues after various treatments (n = 3). *$P < 0.05$; **$P < 0.01$. (**g**) H&E stained images of the heart after various administrations. Scale bars are 50 μm. The black arrows point to dead cells.

pharmacokinetics studies were conducted on the mice treated with BDDF NPs and free DOX to evaluate plasma DOX levels at various time points postinjection (Figure 5a and Table S1). The blood circulation half-lives of BDDF NPs and free DOX were 17.69 and 2.42 h, respectively. The half-life of BDDF NPs was more than 8-fold that of DOX, indicating that BDDF NPs could effectively prolong the blood circulation time of DOX. NIR imaging revealed that BDDF NPs were metabolized via the hepato-gastrointestinal pathway. LPO levels in the tumor tissues were detected (Figure 5d). LPO content increased with postinjection time in both free DOX and BDDF NP groups. These data suggested that the Fe^{2+}-coordinated BDDF NPs could maintain the Fenton reaction of Fe^{2+} and increase ROS to elevate LPO levels.

Synergistic Antitumor Effect of BDDF NPs

U87MG tumor-bearing mice were used to evaluate the synergistic antitumor effect of BDDF NPs. All the mice were randomly divided into three groups, and various treatments were administered intravenously. Tumor size and body weight were tested every other day. The results are shown in Figures 6a and d, S8. BDDF NPs resulted in a higher tumor inhibition rate (70.7%) than free DOX (55.4%) after treatment 30 days, primarily because they targeted tumors, had a long circulation time, and accumulated in tumors. In addition, the BDDF NP groups did not experience body weight loss and presented significantly extended survival times (Figure 6b and c). The body weight of the mice in the free DOX group decreased due to the severe toxic side effects of DOX. Images of tumor sections subjected to terminal deoxynucleotidyl transferase nick-end labeling (TUNEL) staining are displayed in Figure 6e and f. The BDDF NP groups showed strong green fluorescence, and the percentages of apoptotic/necrotic cells calculated by ImageJ based on the TUNEL staining images were 0.18% (control), 41.2% (DOX), and 62.8% (BDDF NPs). Representative liver, heart,

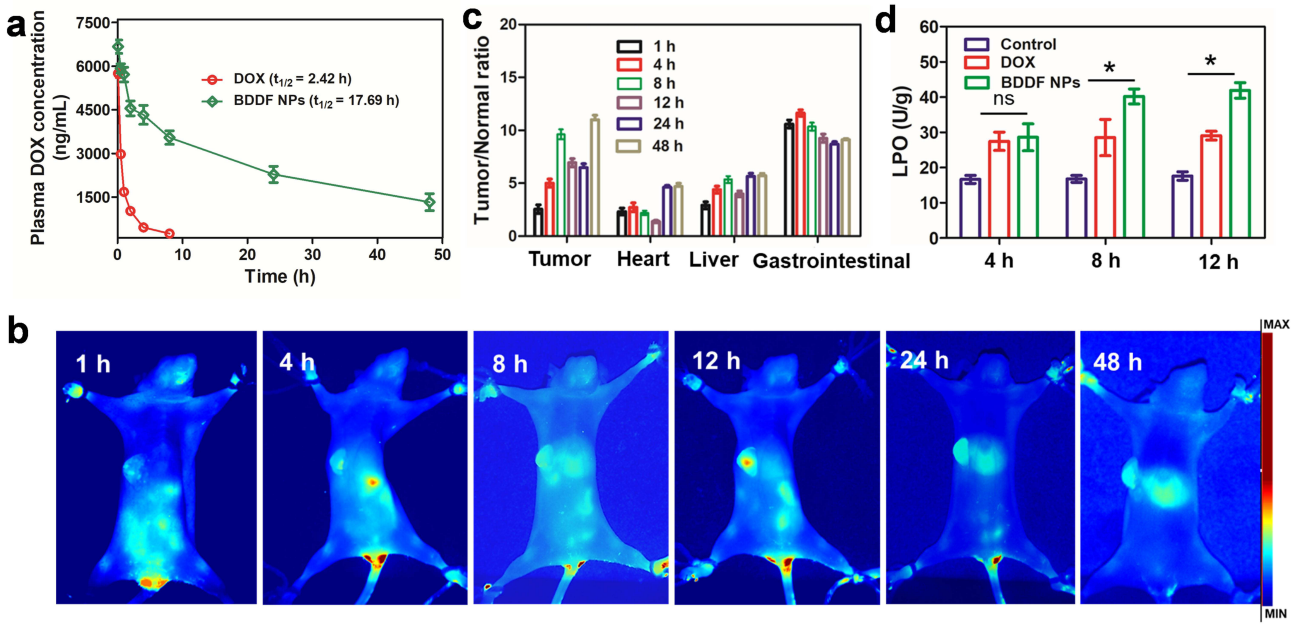

Figure 5 In vivo NIR optical imaging and pharmacokinetic study. (**a**) Pharmacokinetics of free DOX, BDDF NPs by measuring plasma DOX concentration in mice (n = 4). (**b**) In vivo NIR fluorescence images of U87MG tumor-bearing mice at 1, 4, 8, 12, 24, and 48 h postinjection of ICG-labelled BDDF NPs intravenously. (**c**) Biodistribution of BDDF NPs by the region of interest (ROI) analysis of NIR images. n = 4, mean ± s.d. (**d**). The tumor tissues of LPO level (n = 3), *P < 0.05.

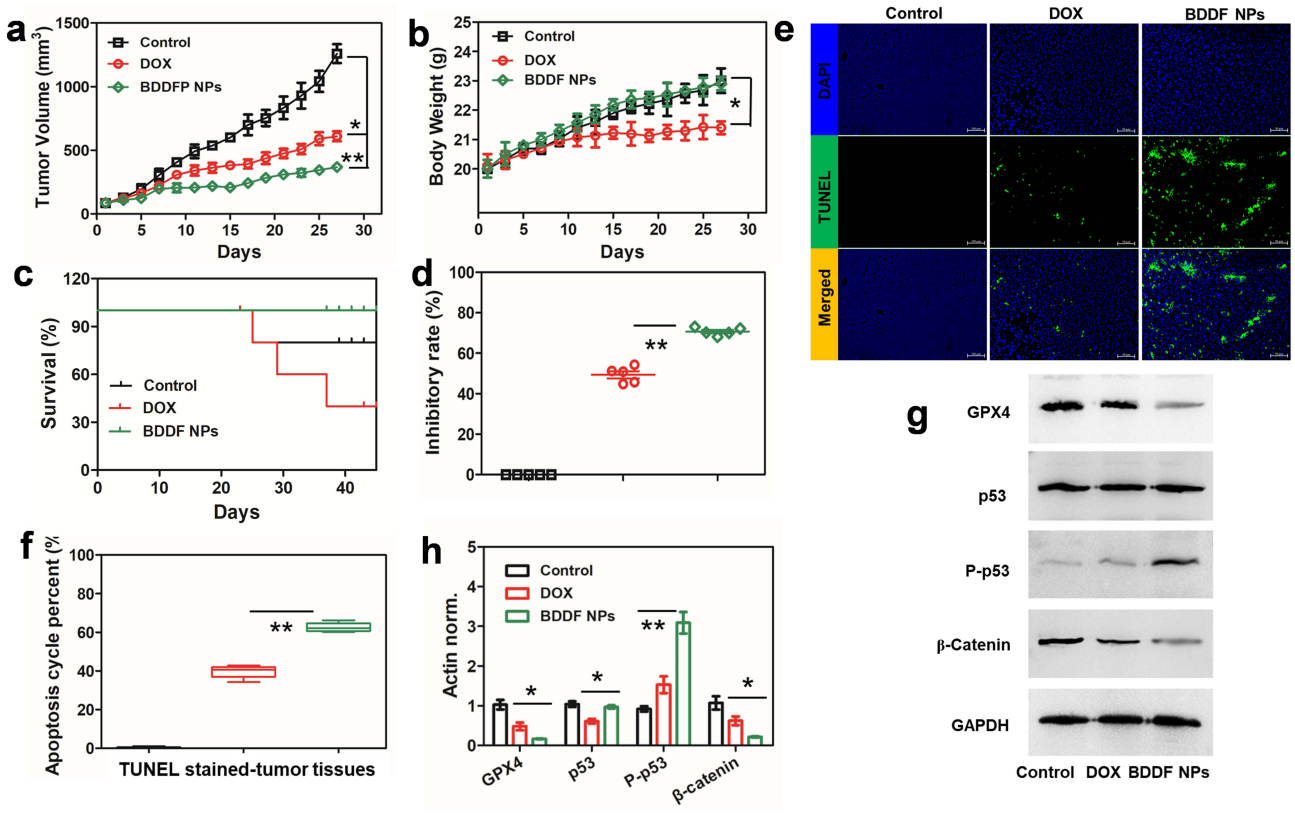

Figure 6 In vivo antitumor evaluation. (**a**) U87MG tumor growth curves, (**b**) body weight, (**c**) survival curve, and (**d**) tumor growth inhibition rates with various treatments (n = 5). *P < 0.05; **P < 0.01. (**e** and **f**) Tumor tissue images were taken using a TUNEL assay under various treatments. Scale bars are 100 μm. (**g** and **h**) Under various treatments, the tumor tissue Western blotting results of GPX4, p53, P-p53, and β-Catenin expression. *P < 0.05; **P < 0.01. Scale bars are 50 μm.

https://doi.org/10.2147/IJN.S461774 DovePress

and tumor tissue sections from various treatment groups were provided in Figure S9. In contrast to those from the free DOX group, the tumor tissues from the BDDF NP group had numerous dead cells, blank spots, and necrosis, suggesting effective synergistic tumor therapy. The liver and heart sections from the free DOX group showed slight myocardial necrosis.

GPX4, β-catenin, P-p53, and p53 protein expression levels were determined through Western blot analysis (Figure 6g and h). Free DOX could enhance the protein expression levels of β-catenin and inhibit those of P-p53 and p53. However, in the BDDF NP group, the protein expression levels of P-p53 and p53 were up-regulated, whereas those of GPX4 and β-catenin were inhibited. All results indicated that the DNA nanodrug delivery system based on tumor telomerase-targeting BDDF NPs and Fe^{2+} coordination had two synergistic antitumor pathways: Fe^{2+}-mediated ferroptosis and the β-catenin/p53 pathway.

Discussion

Studies have shown that nanodrug delivery systems exhibit high drug loading, passive targeting (EPR effect), and suitable pharmacokinetic parameters in vivo, and they can integrate diagnosis and treatment.[36,37] In this study, we exploited biocompatible telomerase-targeting hairpin DNA enriched with Fe^{2+} in their A base pairs to design a DOX carrier to assemble BDDF NPs through a clever tailor-made process. Meanwhile, BDDF NPs acted as the molecular core.[18] The main components of these circular-like shape nanoparticles are the telomerase-targeting hairpin DNA and therapeutic agent DOX. It does not need other delivery materials, thus reducing the toxic side effects induced by the drug carrier. Here, we demonstrate that the Fe^{2+}-DNA @DOX structure targets telomerase in tumors, reduces DOX-mediated cardiotoxicity, and exhibits long circulation times and highly synergistic antitumor effects.

Telomerase is overexpressed in numerous human cancer cells.[38,39] It plays a crucial role in tumor cell division. By contrast, telomerase is nearly absent from normal cells. Therefore, telomerase has long been used as an antitumor therapy and diagnostic target.[40,41] In this work, we proved that telomerase activities were high in glioma U87MG cells and minimal in AC16 normal cells (Figure 2e). Therefore, as revealed by NIR images, BDDF NPs were extensively taken up by U87MG cells and showed strong targeting ability. The NIR fluorescence signal of BDDF NPs in tumor tissues was more robust than that in all the other organs at 12 h and persisted at 48 h, indicating a good targeting ability associated with the high telomerase activities in U8MG cells. Another interesting finding was the prolonged blood circulation times and tumor accumulation of BDDP NPs.

This work primarily aims to utilize different telomerase activities and iron-increased demand in tumor and normal cells to reduce DOX-mediated cardiotoxicity and achieve synergistic therapy. BDDF NPs showed low toxicity against normal cells with low telomerase activities and iron dependency.[31,39] Consequently, they demonstrated limited retention in heart tissues and attenuated severe DOX-mediated cardiotoxicity. At the same time, the relevant mechanism of this effect was investigated. In vitro and in vivo studies revealed that BDDF NPs could reduce DOX-mediated cardiotoxicity by enhancing SOD activities and HO-1 protein expression.[42] In vitro studies on synergistic antitumor effects indicated that the BDDF NPs induced remarkable cell necrosis (Q4) compared with DOX. The same effect was observed in in vivo studies. The tumor inhibition rate of BDDF NPs was higher than that of DOX. In vitro and in vivo Western blot analysis demonstrated that the GPX4/β-catenin proteins were down-regulated and the P-p53/p-53 proteins were up-regulated. These effects were accompanied by increased LPO content in tumor cells and tissues. The impressive therapeutic efficacy of BDDF NPs may be attributed to the following: tumor cells are more vulnerable to iron-catalyzed ferroptosis, then the Fe^{2+}-based DNA drug delivery system releases additional Fe^{2+} to activate the ferroptosis pathway in tumor cells/tissues. This pathway assisted the killing of tumor cells via the β-catenin/p53 pathway.

Conclusion

In this work, we exploited the synergistic effect of nanoparticles, namely, the coordination between Fe^{2+} and hairpin DNA, to coordinate DOX in cores via self-assembly. In vitro studies revealed that the nanoparticles had a preferable size of 61.2 ± 7 nm and a reasonable drug release rate. In vitro and in vivo studies showed that the targeting ability of BDDF NPs was conferred by hairpin DNA that targeted tumor cell/tissue telomerase and led to the long blood circulation and tumor accumulation time of BDDF NPs. BDDF NPs could significantly reduce DOX's cardiomyocyte and cardiac toxicity by improving the antioxidation system and targeting abilities. The mechanism of the synergistic antitumor effect of BDDF NPs mainly involved two pathways: ferroptosis and the β-catenin/p53 pathway. Our therapeutic nanoparticles

can be considered DNA-targeting DOX carriers with a solid synergistic antitumor effect, minor cardiotoxicity, and ability for targeted tumor delivery, thus representing a material with great potential for clinical cancer therapy.

Acknowledgments

We gratefully acknowledge support from the Program of AnHui for International Cooperation projects (202104b11020017) and Overseas Students Innovation Merit-based Plan Project (20221CX034). Youth fund of Natural Science Foundation of Anhui Province (2208085QH261). Higher Education Science Research Project of Anhui Province (2022AH051362). Scientific research platform of Suzhou University (2021XJPT33, 2021XJPT37ZC). Research Foundation for Ph. D. of Suzhou University (2021BSK048, 2021BSK021) and Key natural scientific research projects of Suzhou University (2023yzd02).

Author Contributions

All authors made a significant contribution to the work reported, whether that is in the conception, study design, execution, acquisition of data, analysis, and interpretation, or all these areas; took part in drafting, revising, or critically reviewing the article; gave final approval of the version to be published; have agreed on the journal to which the article has been submitted; and agree to be accountable for all aspects of the work.

Disclosure

The authors declare no competing financial interest.

References

1. Bonvalot S, Pechoux CL, Baere TD, et al. First-in-human study testing a new radioenhancer using nanoparticles (NBTXR3) activated by radiation therapy in patients with locally advanced soft tissue sarcomas. *Clinical Trial Clin Cancer Res*. 2017;23(4):908–917. doi:10.1158/1078-0432.CCR-16-1297
2. Phillips E, Penate-Medina O, Zanzonico PB, et al. Clinical translation of an ultrasmall inorganic optical-PET imaging nanoparticle probe. *Clinical Trial Sci Transl Med*. 2014;6(260). doi:10.1126/scitranslmed.3009524
3. Liu SB, Shang YX, Jiao YF, et al. DNA-based plasmonic nanostructures and their optical and biomedical applications. *Nanotechnology*. 2021;32(40):402002. doi:10.1088/1361-6528/ac0d1c
4. Hu QQ, Li H, Wang LH, et al. DNA nanotechnology-enabled drug delivery systems. *Chem Rev*. 2019;119(10):6459–6506. doi:10.1021/acs.chemrev.7b00663
5. Vries JW, Schnichels S, Hurst J, et al. DNA nanoparticles for ophthalmic drug delivery. *Biomaterials*. 2018;157:98–106. doi:10.1016/j.biomaterials.2017.11.046
6. Etter EL, Mei KC, Nguyen J. Delivering more for less: nanosized, minimal-carrier and pharmacoactive drug delivery systems. *Adv Drug Deliv Rev*. 2021;179:113994. doi:10.1016/j.addr.2021.113994
7. Zhang C, Li X, Tian C, et al. DNA nanocages swallow gold nanoparticles (AuNPs) to form AuNP@DNA cage core-shell structures. *ACS Nano*. 2014;8(2):1130–1135. doi:10.1021/nn406039p
8. Kahn JS, Freage L, Enkin N, et al. Stimuli-Responsive DNA-functionalized metal-organic frameworks (MOFs). *Adv Mater*. 2017;29(6):120–134. doi:10.1002/adma.201602782
9. Bravo-Anaya L, Fernández-Solís K, Rosselgong J, et al. Chitosan-DNA polyelectrolyte complex: influence of chitosan characteristics and mechanism of complex formation. *Int J Biol Macromol*. 2019;126:1037–1049. doi:10.1016/j.ijbiomac.2019.01.008
10. Shi BY, Zheng M, Tao W, et al. Challenges in DNA delivery and recent advances in multifunctional polymeric DNA delivery systems. *Biomacromolecules*. 2017;18(8):2231–2246. doi:10.1021/acs.biomac.7b00803
11. Yang GQ, Cai WB, Zhang ZW, et al. Progress in programmable DNA-aided self-assembly of the master frame of a drug delivery system. *ACS Appl Bio Mater*. 2023;6(12):5125–5144. doi:10.1021/acsabm.3c00636
12. Confederat S, Sandei I, Mohanan G, et al. Nanopore fingerprinting of supramolecular DNA nanostructures. *Biophys J*. 2022;121(24):4882–4891. doi:10.1016/j.bpj.2022.08.020
13. Harley CB. Telomerase and cancer therapeutics. *Nat Rev Cancer*. 2008;8(3):167–179. doi:10.1038/nrc2275
14. Bajaj S, Kumar MS, Peters GJ, et al. Targeting telomerase for its advent in cancer therapeutics. *Med Res Rev*. 2020;40(5):1871–1919. doi:10.1002/med.21674
15. Zhou WH, Saran RJ, Liu JW. Metal Sensing by DNA. *Chem Rev*. 2017;117(12):8272–8325. doi:10.1021/acs.chemrev.7b00063
16. Wang MF, Tsukamoto M, Sergeyev VG, et al. Metal ions sensing by biodots prepared from DNA, RNA, and nucleotides. *Biosensors*. 2021;11(9):333. doi:10.3390/bios11090333
17. Li MY, Wang CL, Di ZH, et al. Engineering multifunctional DNA hybrid nanospheres through coordination-driven self-assembly. *Angew Chem Int Ed Engl*. 2019;58(5):1350–1354. doi:10.1002/anie.201810735
18. Ouameur AA, Arakawa H, Ahmad R, et al. A Comparative study of Fe(II) and Fe(III) interactions with DNA duplex: major and minor grooves bindings. *DNA Cell Biol*. 2005;24(6):394–401. doi:10.1089/dna.2005.24.394
19. Jiang K, Chen YS, Zhao D, et al. A facile and efficient approach for hypertrophic scar therapy via DNA-based transdermal drug delivery. *Nanoscale*. 2020;12(36):18682–18691. doi:10.1039/d0nr04751a

20. Mei L, Zhu GZ, Qiu LP, et al. Self-assembled multifunctional DNA nanoflowers for the circumvention of multidrug resistance in targeted anticancer drug delivery. *Nano Res*. 2015;8(11):3447–3460. doi:10.1007/s12274-015-0841-8
21. Halley PD, Lucas CR, McWilliams EM, et al. Daunorubicin-loaded DNA origami nanostructures circumvent drug-resistance mechanisms in a leukemia mode. *Small*. 2016;12(3):308–320. doi:10.1002/smll.201502118
22. Ma Y, Wang ZH, Zhang M, et al. A telomerase-specific doxorubicin-releasing molecular beacon for cancer theranostics. *Angew Chem Int Ed Engl*. 2016;55(10):3304–3308. doi:10.1002/anie.201509182
23. Liu B, Zhang JF, Li LL. Metal-DNA coordination-driven self-assembly: a conceptual methodology to expand the repertoire of DNA nanobiotechnology. *Chemistry*. 2019;25(59):13452–13457. doi:10.1002/chem.201902501
24. Ge ZL, Guo LJ, Wu GQ, et al. DNA origami-enabled engineering of ligand-drug conjugates for targeted drug delivery. *Small*. 2020;16(16):e1904857. doi:10.1002/smll.201904857
25. Yao C, Ou JH, Tang JP, et al. DNA supramolecular assembly on micro/nanointerfaces for bioanalysis. *Acc Chem Res*. 2022;55(15):2043–2054. doi:10.1021/acs.accounts.2c00170
26. Li Y, Yang PH, Lei N, et al. Assembly of DNA-templated bioluminescent modules for amplified detection of protein biomarkers. *Anal Chem*. 2018;90(19):11495–11502. doi:10.1021/acs.analchem.8b02734
27. Shani L, Michelson AN, Minevich B, et al. DNA-assembled superconducting 3D nanoscale architectures. *Nat Commun*. 2020;11(1):5697. doi:10.1038/s41467-020-19439-9
28. Huang HM, Stephan P, Kries H. Engineering DNA-Templated Nonribosomal Peptide Synthesis. *Cell Chem Biol*. 2021;28(2):221–227.e7. doi:10.1016/j.chembiol.2020.11.004
29. Ye JJ, Weichelt R, Kemper U, et al. Casting of gold nanoparticles with high aspect ratios inside DNA molds. *Small*. 2020;16(39):e2003662. doi:10.1002/smll.202003662
30. Liu B, Hu F, Zhang JF, et al. A biomimetic coordination nanoplatform for controlled encapsulation and delivery of drug-gene combinations. *Angew Chem Int Ed Engl*. 2019;58(26):8804–8808. doi:10.1002/anie.201903417
31. Hassannia B, Vandenabeele P, Berghe TV. Targeting ferroptosis to iron out cancer. *Cancer Cell*. 2019;35(6):830–849. doi:10.1016/j.ccell.2019.04.002
32. Shan LL, Huo YL, Li SY, et al. Geraniin-based self-assemble nanoplatform for antioxidation reduced cardiotoxicity and tumor synergistic therapy. *J Biomed Nanotechnol*. 2023;19(5):758–769. doi:10.1166/jbn.2023.3580
33. Shan LL, Gao GZ, Wang W, et al. Self-assembled green tea polyphenol-based coordination nanomaterials to improve chemotherapy efficacy by inhibition of carbonyl reductase 1. *Biomaterials*. 2019;210:62–69. doi:10.1016/j.biomaterials.2019.04.032
34. Dixon SJ, Lemberg KM, Lamprecht MR, et al. Ferroptosis: an iron-dependent form of nonapoptotic cell death. *Cell*. 2012;149(5):1060–1072. doi:10.1016/j.cell.2012.03.042
35. Vishwakarma K, Dey R, Bhatt H. Telomerase: a prominent oncological target for development of chemotherapeutic agents. *Eur J Med Chem*. 2023;249:115121. doi:10.1016/j.ejmech.2023.115121
36. Xu WJ, Lin ZX, Pan SJ, et al. Direct assembly of metal-phenolic network nanoparticles for biomedical applications. *Angew Chem Int Ed Engl*. 2023;62(45):e202312925. doi:10.1002/anie.202312925
37. Farjadian F, Ghasemi A, Gohari O, et al. Nanopharmaceuticals and nanomedicines currently on the market: challenges and opportunities. *Nanomedicine (Lond)*. 2019;14(1):93–126. doi:10.2217/nnm-2018-0120
38. Lansdorp PM. Telomeres, Telomerase and Cancer. *Arch Med Res*. 2022;53(8):741–746. doi:10.1016/j.arcmed.2022.10.004
39. Sugarman ET, Zhang G, Shay JW. In perspective: an update on telomere targeting in cancer. *Mol, Carcinog*. 2019;58(9:1581–1588. doi:10.1002/mc.23035.
40. Elisa A, Lauren K, Wen PY, et al. Telomerase as a therapeutic target in glioblastoma. *Neuro Oncol*. 2021;23(12):2004–2013. doi:10.1093/neuonc/noab203
41. Meyerson M. Role of telomerase in normal and cancer cells. *J Clin Oncol*. 2000;18(13):2626–2634. doi:10.1200/JCO.2000.18.13.2626
42. Syahputra RA, Harahap U, Dalimunthe A, et al. Protective effect of Vernonia amygdalina delile against doxorubicin-induced cardiotoxicity. *Heliyon*. 2021;7(7):e07434. doi:10.1016/j.heliyon.2021.e07434